Comparison of Solid and Perforated Hybrid Precast Concrete Shear Walls for Seismic Regions

B. J. Smith,[1] Y. C. Kurama,[2] and M. J. McGinnis[3]

[1]Civil Engineering and Geological Sciences, Univ. of Notre Dame, 156 Fitzpatrick Hall, Notre Dame, IN 46556; PH: (574) 631-5380; email: bsmith24@nd.edu
[2]Civil Engineering and Geological Sciences, Univ. of Notre Dame, 156 Fitzpatrick Hall, Notre Dame, IN 46556; PH: (574) 631-8377; email: ykurama@nd.edu
[3]Civil Engineering, University of Texas at Tyler, 3900 University Blvd, Tyler, TX 75799; PH: (903) 565-5870; email: mmcginnis@uttyler.edu

ABSTRACT

This paper compares the measured lateral load behaviors of two 0.4-scale "hybrid" precast concrete wall test specimens – one wall with solid panels and the other with perforated panels. The test specimens have the same overall geometry and utilize a combination of mild [i.e., Grade 400 (U.S. Grade 60)] steel and high-strength unbonded post-tensioning (PT) steel for lateral resistance across horizontal joints. The mild steel reinforcement is designed to yield in tension and compression, providing energy dissipation. The unbonded PT steel provides self-centering capability, reducing the residual lateral displacements of the wall after a large earthquake. The comparisons between the two walls focus on the applied lateral load versus displacement behavior, energy dissipation, shear deformations, and behavior along the critical horizontal base-panel-to-foundation joint. Both specimens demonstrated excellent re-centering and energy dissipation capabilities as well as ductile behavior over lateral displacements at or greater than the ACI ITG-5.1 (2007) requirement. The perforated specimen was able to achieve greater lateral drift due to improvements made to the details of the panel reinforcement at the wall toes. Ultimately, these results are expected to support the successful code approval of hybrid precast shear walls for moderate and high seismic regions of the United States.

INTRODUCTION AND BACKGROUND

As described in Smith et al. (2011a), the hybrid precast wall system investigated in this research utilizes a combination of mild [i.e., Grade 400 (U.S. Grade 60)] steel bars and high-strength unbonded post-tensioning (PT) strands for lateral resistance across horizontal joints. Under the application of lateral loads into the nonlinear range, the primary mode of displacement in these walls occurs through gap opening at the horizontal joint between the base panel and the foundation, allowing the wall to undergo large lateral displacements with little damage. Upon unloading, the PT steel provides a restoring force to close this gap, thus reducing the residual lateral displacements of the wall after a large earthquake. The use of unbonded tendons delays the yielding of the PT strands and reduces the tensile stresses transferred to the

concrete (thus reducing cracking) as the tendons elongate under lateral loading. The mild steel bars crossing the base joint are designed to yield in tension and compression, providing energy dissipation through the gap opening/closing behavior. A pre-determined length of these energy dissipating bars (or E.D. bars) is unbonded at the bottom of the base panel (by wrapping the bars with plastic sleeves) to reduce the steel strains and prevent low-cycle fatigue fracture.

The hybrid precast wall system offers high quality production, relatively simple construction, and excellent seismic characteristics by providing self-centering to the building as well as energy dissipation to control the lateral displacements. Despite these desirable characteristics, hybrid precast walls are classified as non-emulative structures since they do not emulate the behavior of conventional cast-in-place reinforced concrete walls. Thus, experimental validation is required by ACI 318 (2008) and ACI ITG-5.1 (2007) prior to their use in seismic regions of the United States. To date, limited tests and analytical studies are available [(Smith et al. (2011a), Rahman and Restrepo (2000), Holden et al. (2001), Kurama (2002), Kurama (2005)]; however, these studies have not generated the required experimental data to satisfy the ACI ITG-5.1 validation criteria. Furthermore, concrete shear walls often feature perforations to allow for windows and doors to be incorporated into the building system. Previous research on perforated precast concrete walls is extremely limited [Allen and Kurama (2002), Mackertich and Aswad (1997)], and there are currently no results published on hybrid walls with perforations. This paper focuses on these important knowledge gaps.

TEST SET-UP AND SPECIMEN PROPERTIES

The test set-up and procedure conformed to the requirements of ACI ITG-5.1. Each wall specimen, referred to as Specimens HW3 (solid wall) and HW4 (perforated wall), was designed based on a 4-story prototype wall within a prototype parking garage structure located in Los Angeles, CA. The specimen design satisfied the guidelines and requirements of ACI ITG-5.2 (2009), ACI-318, and ASCE 7 (2005). Schematic drawings of the test set-up and specimen cross-section (depicting the confinement steel geometry) are shown in Figure 1. More information on the overall design of the walls can be found in Smith and Kurama (2009) and Smith et al. (2011a). A detailed discussion of the design of the panel perforations can be found in Smith et al. (2011b).

Each test was conducted at 0.40-scale, which satisfies the minimum scaling limit of ACI ITG-5.1. The specimens featured two wall panels: the base panel representing the 1st story of the structure and the upper panel representing the 2nd through 4th stories, thereby satisfying the ACI ITG-5.1 requirement for testing multi-panel walls (such that an upper panel-to-panel joint as well as the base-panel-to-foundation joint are evaluated). The 0.40-scale wall length, l_w, was 243 cm (96 in.), base panel height, h_{pb}, was 145 cm (57.5 in.), and wall thickness, t_w, was 15.9 cm (6.25 in.). It was possible to test the upper story panels of the 4-story prototype wall as a single panel since the joints between the upper panels were designed to have no nonlinear behavior and no gap opening. The lateral load was applied 3.66 m (12 ft) from the wall base (near the resultant location of the 1st mode inertial forces),

resulting in a wall base moment to shear ratio of $M_b/V_b=1.5l_w$. An external downward axial load of about 325 kN (73 kips) was applied at the center of the top of each specimen to simulate the service-level tributary gravity loads acting on the prototype structure during an earthquake (assumed to be 1.0 times the service gravity load plus 0.25 times the unreduced service live load).

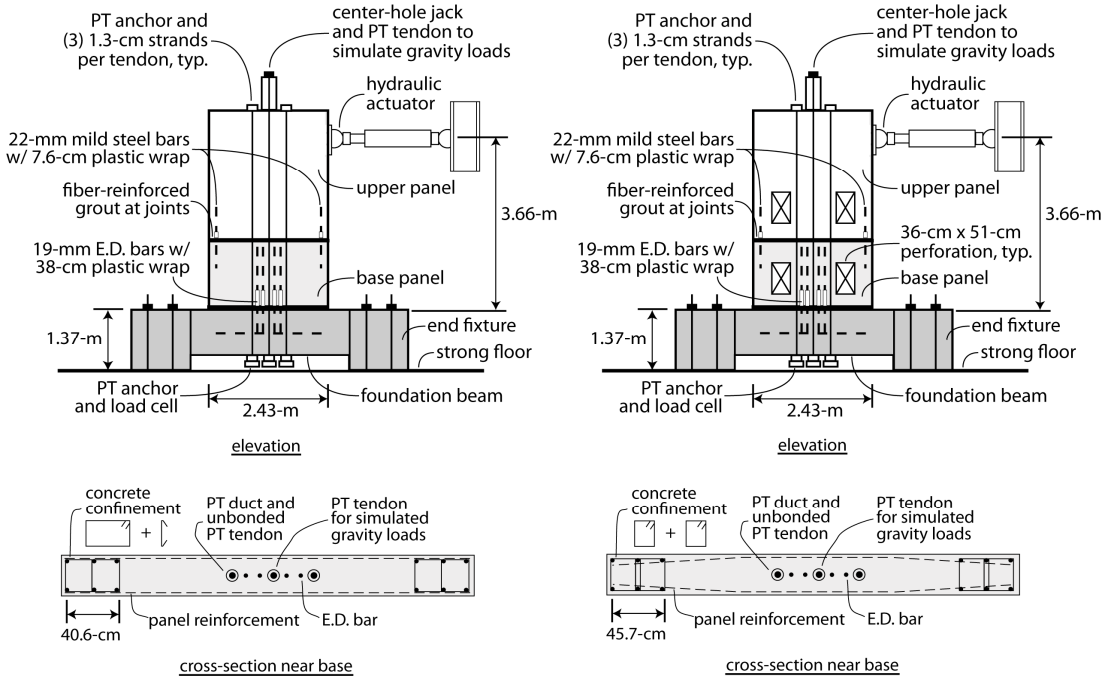

Figure 1. Test configuration and specimen details: (a) HW3 (solid wall); (b) HW4 (perforated wall).

For both specimens, the location and material properties of the PT and E.D. steel were the same. The PT steel consisted of two tendons located 28 cm (11 in.) north and south from the wall centerline. The tendons were placed near the wall centerline to reduce the strand strains and also keep the PT ducts away from the critical confined toe regions of the wall. Each tendon contained three 1.3-cm diameter (0.5-in.) strands [design ultimate strength, f_{pu}=1862 MPa (270 ksi)] with an unbonded length from the top of the wall to the bottom of the foundation beam of approximately 5.5 m (18 ft). The average initial tendon stress, calculated from the measured individual strand forces prior to the application of the lateral load, was $f_{pi}=0.54f_{pu}$. The E.D. steel crossing the base joint consisted of four 19-mm diameter (U.S. No. 6) bars [measured yield strength, f_{sy}=448 MPa (65 ksi), and yield strain, ε_{sy}=0.0023 cm/cm], with one pair of bars placed 19 cm (7.5 in.) north and south from the wall centerline and the other pair 8.9 cm (3.5 in.) north and south from the centerline. The E.D. bars were unbonded over a length of 38 cm (15 in.) at the bottom of the base panel. Across the upper panel-to-panel joint, only two 22-mm (U.S. No. 7) diameter bars were used, with one bar located 10 cm (4.0 in.) from each end of the wall. This reinforcement was designed not to yield; thereby limiting any gap opening along this joint. To prevent strain concentrations in the panel-to-panel joint reinforcement, a short 7.6 cm length (3.0 in.) of the bars was unbonded at the bottom

of the upper panel. The design unconfined concrete strength for the walls was 41 MPa (6.0 ksi) and the design confined concrete strength (at the toes of the base panel) was 62 MPa (9.0 ksi). On the day each wall was tested, the measured unconfined concrete strength for the base panel was 55 MPa (8.0 ksi) for Specimen HW3 and 50 MPa (7.3 ksi) for Specimen HW4. At the horizontal joints, fiber-reinforced grout (with polypropylene microfilament fibers at 0.065% by volume) was used. The test-day strength of the base joint grout was 58 MPa (8.4 ksi) for both the solid and perforated walls.

As shown in Figure 1b, the panels of Specimen HW4 featured two rectangular openings, each with a length, l_o, of 36 cm (14 in.) and a height, h_o, of 51 cm (20 in.). The perforations were placed in a symmetrical layout with respect to the wall centerline, with the exterior edges of the perforations located 51 cm (20 in.) from the panel edge and 36 cm (14 in.) from the panel base. The perforations in the upper panel represented those in the 2nd story. The perforations in the 3rd and 4th stories of the prototype wall were not modeled since they would be less critical than the lower story perforations.

Based on the observed performance of the Specimen HW3 (discussed in more detail later in the paper), the concrete confinement detailing at the toes of the structure was modified in the Specimen HW4. Figure 1a depicts the confinement reinforcement in Specimen HW3, which consisted of a large hoop [11.4 cm (4.5 in.) by 40.6 cm (16 in.)] with an intermediate crosstie located at the mid-length of the hoop. The confinement hoop and crosstie spacing was 7.6 cm (3.0 in.). The horizontal distributed 10-mm (U.S. No. 3) deformed bars at each face of the base panel were placed outside of the confinement cages for ease of construction. As shown in Figure 1b, the confinement reinforcement in Specimen HW4 was modified to consist of two smaller hoops [each 11.4 cm (4.5 in.) by 25.4 cm (10 in.)] that were overlapped to create a larger overall confinement steel geometry [11.4 cm (4.5 in.) by 45.7 cm (18 in.)]. This modification was made primarily to reduce confined concrete damage, which partially resulted from bowing-out of the longer legs of the bottom hoops observed in the solid specimen (as discussed in more detail later, the cross-ties were not effective in confining the concrete), and secondarily to allow for the entire exterior vertical chord of the perforated base panel to be reinforced. The confinement hoop spacing between the two walls remained the same [7.6 cm (3.0 in.)]. As an additional modification, the horizontal distributed 10-mm (U.S. No. 3) deformed bars were placed inside of the confinement cages in an attempt to limit the concrete cover spalling in the perforated base panel.

MEASURED BEHAVIOR OF SPECIMENS

Figure 2 shows the reversed-cyclic lateral displacement history used in the testing of the wall specimens, with three repeated cycles at each displacement increment. The wall drift, Δ_w (positive with the wall displaced southward), was measured as the relative lateral displacement of the wall between the lateral load location and the foundation divided by the height to the lateral load. For the given wall dimensions, the validation-level drift per ACI ITG-5.1 is Δ_w=2.30% for each specimen. Specimen HW3 was able to sustain two cycles at this validation-level drift

followed by a greater drift cycle of Δ_w=±2.95%. In comparison, Specimen HW4 was able to sustain three cycles at the validation-level drift followed by an additional set of three cycles at a maximum drift of Δ_w=±3.05%.

Figure 3a shows the solid wall specimen at Δ_w=+2.95% (note the gap opening along the base joint at the north end). Minor concrete cracking in the base panel and no cracking in the upper panel was observed (note that the cracks visible in Figure 3 were highlighted with markers during the test for enhanced viewing). Crushing of the confined concrete at the wall toes (see Figure 3b) and slight bowing of the longer legs of the bottom confinement hoops occurred during the large displacement cycles. It was possible for the longer legs of the confinement hoops to bow outwards (which reduced the confinement effectiveness) since the crossties did not directly engage the hoop steel [note that the crossties did engage the longitudinal (vertical) reinforcement within the confinement cages as required by ACI 318]. The total strength loss at the completion of the drift history was less than 20%, thus satisfying the ACI ITG-5.1 validation requirement. Additional loading of the wall beyond the required displacement history resulted in further strength loss and subsequent failure of the specimen due to concrete crushing (defined by ACI ITG-5.1 as the drift at which the total strength loss exceeds 20%). No concrete crushing in the upper panel and no significant gap opening or slip in the upper panel-to-panel joint was observed during the test.

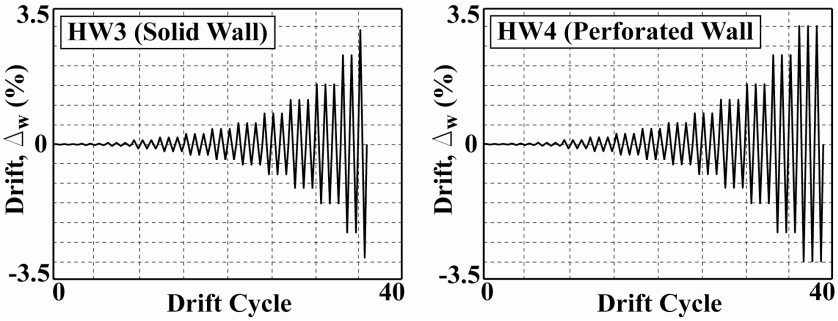

Figure 2. Drift history: (a) HW3; (b) HW4.

Similarly, Figure 3c shows the perforated wall specimen at the third cycle to Δ_w=+3.05%. The total strength loss at the completion of the drift history was less than 20%, thus satisfying the ACI ITG-5.1 requirement for validation. The damage to the wall was mostly concentrated in the base panel, consisting of distributed concrete cracks predominately in the horizontal chord members (both above and below the perforations) and in the center vertical chord (in between the perforations). Limited cracking in the upper panel was also observed, concentrated at the corners of the perforations. In addition, cover spalling was observed at both wall toes; however, crushing of the confined concrete was only beginning to develop during the last set of drift cycles (see Figure 3d). The improved performance of the confined concrete was related to the modifications made to the confinement steel detailing, specifically through the use of two shorter hoops (with length-to-width ratio of 2.22) instead of one long hoop (with length-to-width ratio of 3.56) and an intermediate tie. The reduction in the confinement hoop length-to-width ratio prevented the bowing of the longer hoop legs, resulting in less damage to the confined concrete. Further, terminating the distributed horizontal 10-mm (U.S. No. 3) bars inside the

confinement cages limited the extent of the cover concrete spalling. No concrete crushing in the upper panel and no significant gap opening or slip in the upper panel-to-panel joint was observed during the test.

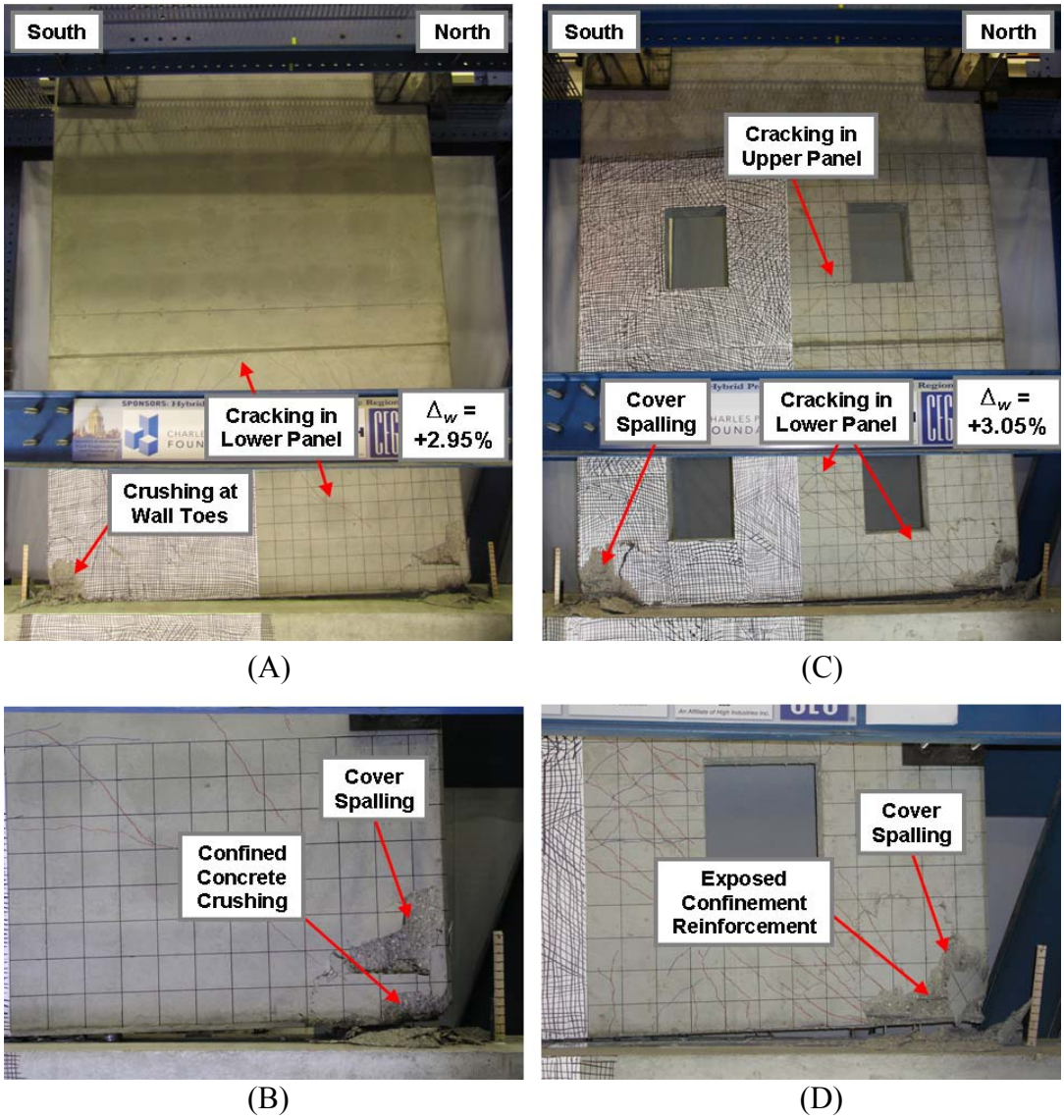

Figure 3. Observed damage: (a) HW3 at third cycle of Δ_w=+2.95%; (b) north end of HW3; (c) HW4 at third cycle of Δ_w=+3.05%; (d) north end of HW4.

Lateral Load Versus Displacement Behavior. Figure 4 compares the measured base shear force, V_b versus wall drift, Δ_w behaviors for the two specimens. The maximum base shear resistance of Specimen HW3 was 551 kN (124 kips) reached at Δ_w=+1.55%, the resistance at the validation-level drift (Δ_w = +2.30%) was 507 kN (114 kips), and the resistance at the final drift cycle (Δ_w=+2.95%) was 443 kN (99.5 kips). For comparison, the maximum base shear resistance of Specimen HW4 was 533 kN (120 kips) reached at Δ_w=+1.55%, the resistance at the validation-level drift (Δ_w = +2.30%) was 528 kN (119 kips), and the resistance at the final drift cycle

(Δ_w=+3.05%) was 432 kN (97.1 kips). Both specimens behaved in a reasonably symmetrical manner in the positive and negative directions, while also exhibiting excellent re-centering capability and energy dissipation. The total strength loss from the maximum base shear resistance to the peak resistance during the final drift cycle for the solid specimen was approximately 19.9% and 13.8% in the positive and negative directions, respectively. For the perforated wall, the total strength losses were approximately 18.9% and 18.7% in the positive and negative directions, respectively. For each specimen, the measured strength and stiffness losses were within the prescribed limitations per ACI ITG-5.1, thereby satisfying the validation criteria. Based on the similarities between the load-displacement behaviors of the two specimens, the presence of the panel openings did not significantly impact the global load-displacement behavior of the wall.

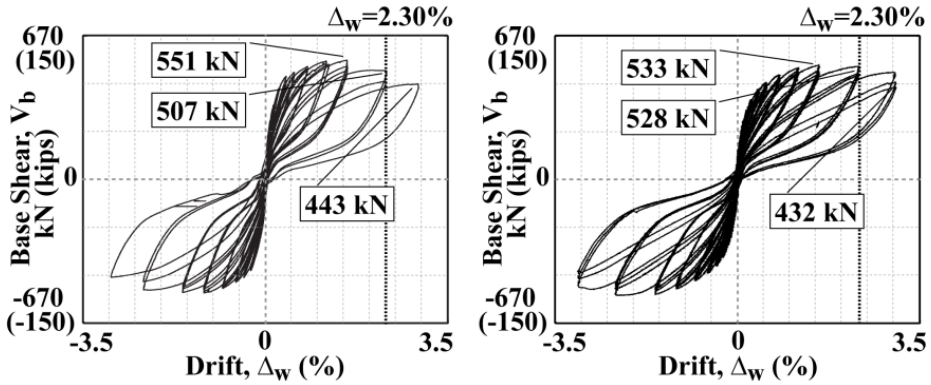

(A) (B)

Figure 4. Base shear force versus wall drift history: (a) HW3 (solid wall); (b) HW4 (perforated wall).

Energy Dissipation. The primary source of energy dissipation in both walls was the yielding of the mild steel reinforcement over the unbonded length of the bars at the base joint. To quantify the amount of energy dissipation, ACI ITG-5.1 uses the energy dissipation ratio, β, which is defined as "the ratio of the measured energy dissipated by the test module during reversing cyclic displacements between given measured drift angles to the maximum theoretical energy that can be dissipated for the same drift angles." ACI ITG-5.1 requires that β be not less than 0.125 at the validation-level drift.

The solid and dashed lines in Figure 5 show the measured energy dissipation ratio, β of Specimens HW3 and HW4, respectively, plotted against the wall drift. The last cycle for each drift level was used to calculate β. It can be seen that both specimens satisfied the ACI ITG-5.1 minimum β requirement at moderate drift levels and continued to exceed the minimum requirement until the end of the test. The perforated wall demonstrated smaller energy dissipation than the solid wall, which

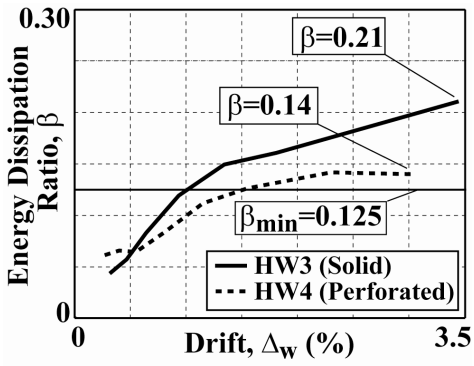

Figure 5. Energy dissipation ratio.

can be attributed to the increased shear deformations of the wall panels and smaller gap opening displacements across the base joint (i.e., vertical size of gap) of the perforated specimen, resulting in less E.D. steel deformations and strains. These differences are discussed in more detail below.

Gap Opening Along Base Joint. As designed, each specimen opened a significant gap along the base-panel-to-foundation joint. The gap opening at the upper panel-to-panel joint was negligible. The vertical gap opening displacements across the base joint were measured using a series of linear variable differential transformers (LVDTs). Figure 6 shows the measured gap opening at the centerline (i.e. mid-length) of the base joint in each wall. It can be seen that at this location, Specimen HW3 formed a larger gap than the Specimen HW4. Since the E.D. bars were located near the wall centerline [±8.9 cm (3.5 in.) and ±19 cm (7.5 in.)], the larger gap opening displacements in the solid specimen resulted in greater E.D. bar deformations, bar strains, and more energy dissipation than in the perforated specimen. The smaller gap opening in the perforated specimen can be partially attributed to the larger shear deformations of the wall panels as discussed below.

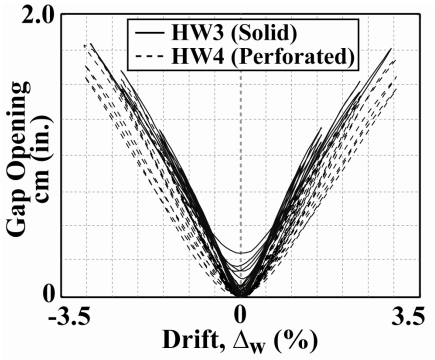

Figure 6. Gap opening along base joint at wall centerline.

Shear Deformations. The solid and dashed lines in Figure 7a show the shear distortion angle, $\tilde{a}$ [calculated as described in Oesterle et al. (1976)] of the base panel measured using two diagonally placed string potentiometers. As may be expected, the shear distortion was considerably greater in the perforated wall as compared to the solid wall; however, for each specimen, the shear distortions were still small despite the relatively low M_b/V_b ratio of $1.5l_w$. This becomes more obvious when, as shown in Figure 7b, the distortion angle of the base panel is plotted as a percentage of the total drift angle to the top of the panel, Δ_{bp} (defined as the relative lateral displacement

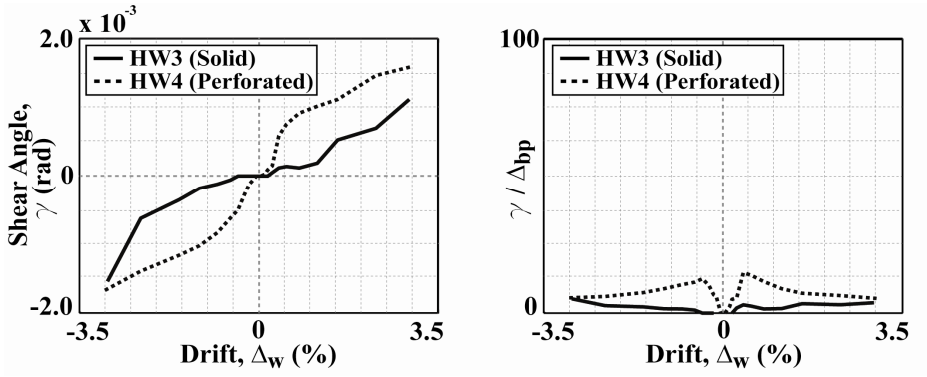

Figure 7. Shear deformations of base panel: (a) shear distortion angle; (b) shear distortion angle normalized by total base panel drift.

between the top of the base panel and the top of the foundation divided by the height of the base panel). It can be seen that neither wall experienced significant shear distortions; and thus, the lateral displacements were governed by rigid body rotations through the gap opening at the base.

Horizontal Slip at Wall Base. The behavior along the base joint was also measured using three-dimensional digital image correlation (3D-DIC), a non-contact optical monitoring technique. The 3D-DIC system measured the in-plane and out-of-plane displacements (within the white-painted regions in Figure 3), providing unprecedented information on the behavior of the walls. By using the 3D-DIC data for the relative horizontal displacements between adjacent points on either side of the base-panel-to-foundation joint, the horizontal slip at the wall base was determined. The solid lines in Figure 8 show the measured base slip at the centerline of Specimen HW3 for loading in the positive and negative directions during the third cycle in each drift series [except for the final drift series where the first cycle (Δ_w=±2.30%) and the third cycle (Δ_w=±2.95%) results are plotted]. Similarly, the dashed lines show the measured slip for Specimen HW4. In general, the slip at the base of both specimens was small, with a maximum slip of about 0.31 cm (0.12 in.) at Δ_w=–2.95% for the solid wall and 0.09 cm (0.04 in.) at Δ_w=+1.55% for the perforated wall. Further, the crushing of the concrete at the wall toes did not result in a disproportionate accumulation of slip. The measured base slip of the perforated wall specimen was less than the maximum allowable slip of 0.15 cm (0.06 in.) per ACI ITG-5.1, thus satisfying this validation criterion. However, the slip in the negative direction for the solid specimen exceeded the maximum allowable value. Since the performance of the solid wall was not negatively affected by the base slip, the current slip limit in ACI ITG-5.1 may be too conservative. The horizontal slip at the upper panel-to-panel joint for both specimens was negligible.

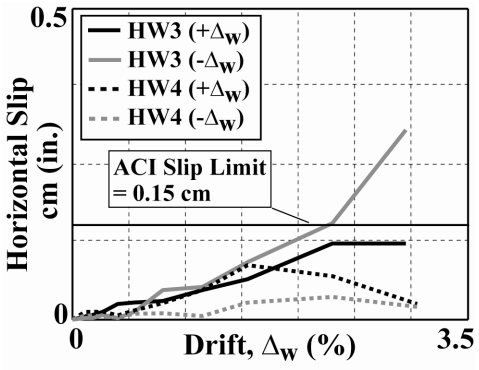

Figure 8. Horizontal slip along base joint.

Neutral Axis Depth. By using the 3D-DIC data for the vertical displacements across the base joint, an estimate for the location of the neutral axis of the section (i.e., "contact length" along the joint) was made. Figure 9 plots the measured neutral axis length at the south end of the two walls, normalized by the wall length. The results are shown for the first cycle in each drift series, except for the last series where all three cycles are shown. During the relatively small displacements, the neutral axis length went through a rapid

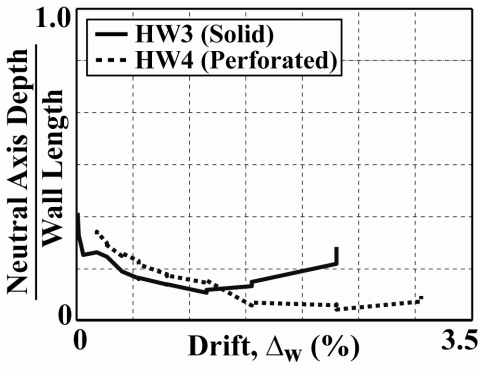

Figure 9. Neutral axis depth along base joint.

decrease associated with gap opening along the joint. As each wall was displaced further, the neutral axis length continued to decrease but at a much slower pace. Once crushing of the confined concrete initiated, the neutral axis length began to elongate to satisfy equilibrium with the reduced concrete stresses. This effect is particularly evident during the final drift series for the solid wall, where bowing of the longer legs of the bottom confinement hoops were observed in addition to the concrete crushing. This trend was less evident in the perforated specimen since less damage to the confined concrete region was observed, likely due to the detailing modifications to the confinement reinforcement.

SUMMARY AND CONCLUSIONS

This paper compares the measured lateral load behavior of a 0.4-scale solid hybrid precast concrete shear wall (Specimen HW3) with the behavior of a similar wall featuring two rectangular perforations in each panel (Specimen HW4). The results demonstrate the potential for the use of hybrid precast concrete walls as special reinforced concrete shear walls in high seismic regions, while also revealing the ability of the system to incorporate panel perforations, a common feature to allow for windows and doors into the building system. The following summary and conclusions can be made based on the experimental results:

- Each wall specimen demonstrated full re-centering capability while also providing large energy dissipation due to the combination of unbonded post-tensioning steel with yielding mild steel reinforcement across the base-panel-to-foundation joint.
- The solid specimen sustained three fully-reversed drift cycles of magnitude equal to or greater than the validation-level drift prescribed by ACI ITG-5.1.
- The damage to the solid wall was limited to the base panel, consisting of the crushing of the confined concrete and minor concrete cracking.
- The perforated specimen sustained three fully-reversed drift cycles at the validation-level drift followed by three additional cycles at a greater drift.
- The damage to the perforated specimen was also concentrated in the base panel, consisting of cover concrete spalling at the wall toes and distributed cracking in the horizontal and vertical chords around the panel perforations. Minor concrete cracking extended into the upper panel, primarily at the corners of the perforations.
- Minor detailing modifications to the confinement reinforcement of the perforated specimen resulted in a considerable improvement in the performance of the confined concrete.
- The panel perforations did not significantly affect the global lateral load versus displacement behavior of the system, since both the solid and perforated walls behaved essentially as a rigid body dominated by gap opening at the base joint.
- The presence of the panel perforations resulted in larger shear deformations of the base panel and smaller gap opening (i.e. vertical displacements) along the

base joint, resulting in a smaller amount of energy dissipation. Both walls satisfied the minimum energy dissipation requirement from ACI ITG-5.1.

- The maximum allowable horizontal slip of 0.15 cm (0.06 in.) prescribed by ACI ITG-5.1 may be too conservative. The measured performance of the solid wall was not negatively affected by measured base slip of up to 0.31 cm (0.12 in.). The concrete crushing at the wall toes did not result in a disproportionate accumulation of slip. The maximum base slip in the perforated wall was smaller than the ACI ITG-5.1 limit.

ACKNOWLEDGEMENTS

This research is funded by the Charles Pankow Foundation and the Precast/Prestressed Concrete Institute (PCI). Additional technical and financial support is provided by the High Concrete Group, LLC, the Consulting Engineers Group, Inc. and the University of Notre Dame. The authors would like to acknowledge the support of the PCI Research and Development Committee as well as the members of the Project Advisory Panel, who include Walt Korkosz (chair) of the Consulting Engineers Group, Inc., Ken Baur of the High Concrete Group, LLC, Neil Hawkins of the University of Illinois at Urbana-Champaign, S.K. Ghosh of S.K. Ghosh Associates, Inc., and Dave Dieter of Mid-State Precast, LP. Additional assistance and material donations have been provided by Jenny Bass of Essve Tech Inc., Randy Draginis and Norris Hayes of Hayes Industries, Ltd., Randy Ernest of Prestress Supply Inc., Eric Fries of Contractors Materials Company, Chris Lagaden of Ecco Manufacturing, Stan Landry of Enerpac Precision SURE-LOCK, Richard Lutz of Summit Engineered Products, Shane Whitacre of Dayton Superior Corporation, and Steve Yoshida of Sumiden Wire Products Corporation. Any opinions, findings, conclusions, and/or recommendations expressed in this paper are those of the authors and do not necessarily represent the views of the above listed individuals or organizations.

REFERENCES

ACI. (2007). “Acceptance Criteria for Special Unbonded Post-Tensioned Precast Structural Walls Based on Validation Testing (ACI ITG-5.1-07) and Commentary.” *ACI Innovation Task Group 5*, Farmington Hills, MI.

ACI. (2008). “Building Code Requirements for Structural Concrete (ACI 318-08) and Commentary.” *ACI Committee 318*, Farmington Hills, MI.

ACI. (2009). “Requirements for Design of a Special Unbonded Post-Tensioned Precast Shear Wall Satisfying ACI ITG-5.1 (ACI ITG-5.2-09) and Commentary.” *ACI Innovation Task Group 5*, Farmington Hills, MI.

Allen, M. and Kurama, Y. (2002). “Design of Rectangular Openings in Precast Walls Under Combined Vertical and Lateral Loads.” *PCI Journal*, 47(2), 58-83.

ASCE. (2005). “Minimum Design Loads for Buildings and Other Structures.” *ASCE/SEI 7-05*, Reston, VA.

Holden, T., Restrepo, J., and Mander J. (2001). "A Comparison of the Seismic Performance of Precast Wall Construction: Emulation and Hybrid Approaches." *Univ. of Canterbury,* Research Report No. 2001-4.

Kurama, Y. (2002). "Hybrid Post-Tensioned Precast Concrete Walls for Use in Seismic Regions." *PCI Journal*, 47(5), 36-59.

Kurama, Y. (2005). "Seismic Design of Partially Post-Tensioned Precast Concrete Walls." *PCI Journal*, 50(4), 100-125.

Mackertich, S., and Aswad, A. (1997). "Lateral Deformations of Perforated Shear Walls for Low and Mid-Rise Buildings." *PCI Journal*, 42(1), 30-41.

Oesterle, R., Fiorato, A., Johal, L., Carpenter, J., Russell, H., and Corley, W. (1976). "Earthquake Resistant Structural Walls - Tests of Isolated Walls." *Portland Cement Association*, Research and Development Report No. 1571, Skokie, IL.

Rahman, A. and Restrepo, J. (2000). "Earthquake Resistant Precast Concrete Buildings: Seismic Performance of Cantilever Walls Prestressed Using Unbonded Tendons." *Univ. of Canterbury,* Research Report No. 2000-5.

Smith, B. and Kurama, Y. (2009). "Design of Hybrid Precast Concrete Walls for Seismic Regions." *Proceeding of the ASCE Structures Congress*, Austin, TX.

Smith, B., Kurama, Y., and McGinnis, M. (2011a). "Design and Measured Behavior of a Hybrid Precast Concrete Wall Specimen for Seismic Regions." *Journal of Structural Engineering*, 137(10), 1052-1062.

Smith, B., Kurama, Y., and McGinnis, M. (2011b). "Design and Measured Behavior of a Perforated Hybrid Precast Concrete Shear Wall for Seismic Regions." *Proceeding of the PCI Annual Convention*, Salt Lake City, UT.